iScience

CellPress
OPEN ACCESS

Article

Acute exposure to artificial light at night alters hippocampal vascular structure in mice

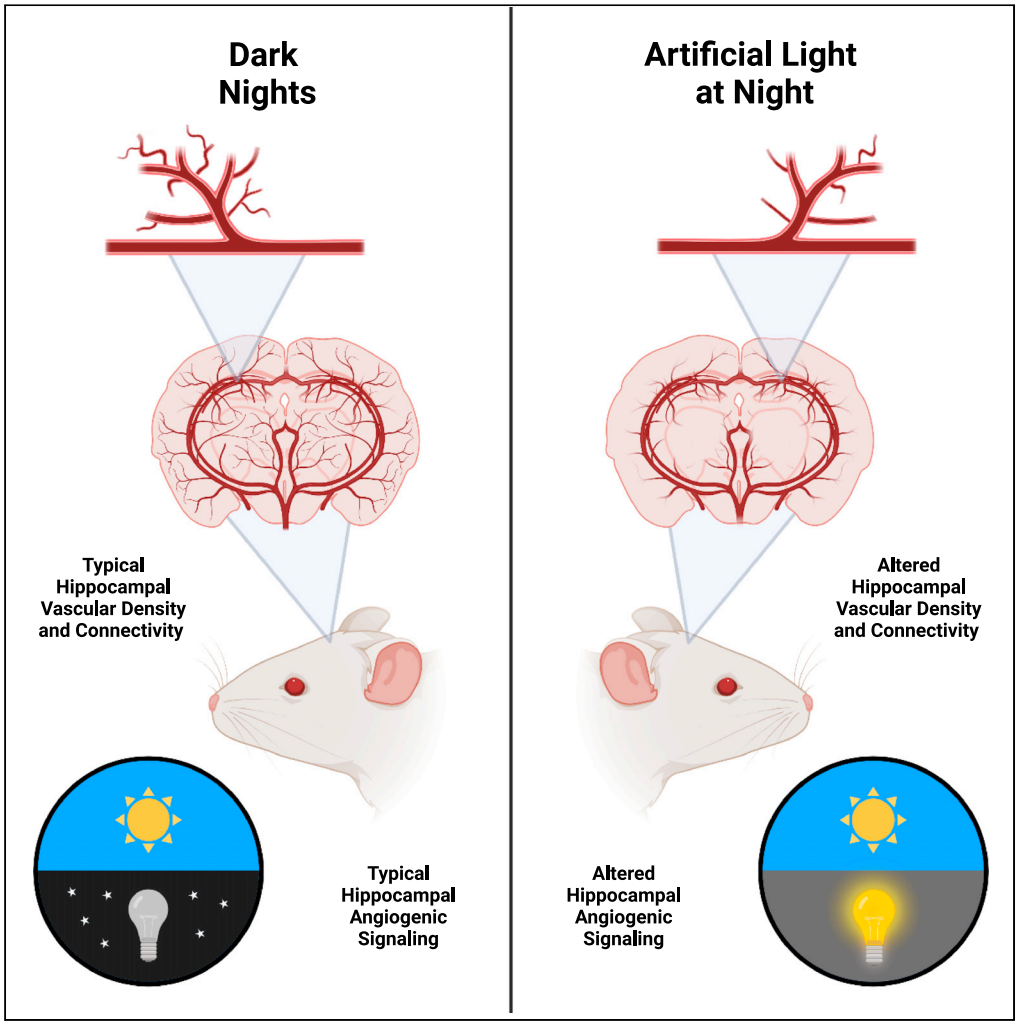

Jacob R. Bumgarner, William H. Walker II, Dominic D. Quintana, ..., James W. Simpkins, A. Courtney DeVries, Randy J. Nelson

jrbumgarner@mix.wvu.edu

Highlights

Artificial light at night (ALAN) is a pervasive and disruptive aspect of modern life

This study examined the effects of acute ALAN exposure on hippocampal vasculature

ALAN exposure altered hippocampal vascular structure and connectivity in mice

Vascular alterations induced by ALAN exposure varied based on sex

Bumgarner et al., iScience 26, 106996
July 21, 2023
https://doi.org/10.1016/j.isci.2023.106996

iScience

CellPress
OPEN ACCESS

Article

Acute exposure to artificial light at night alters hippocampal vascular structure in mice

Jacob R. Bumgarner,[1,4,*] William H. Walker II,[1] Dominic D. Quintana,[1] Rhett C. White,[1] Alexandra A. Richmond,[1] O. Hecmarie Meléndez-Fernández,[1] Jennifer A. Liu,[1] Darius D. Becker-Krail,[1] James C. Walton,[1] James W. Simpkins,[1] A. Courtney DeVries,[1,2,3] and Randy J. Nelson[1]

SUMMARY

The structure and function of the cardiovascular system are modulated across the day by circadian rhythms, making this system susceptible to circadian rhythm disruption. Recent evidence demonstrated that short-term exposure to a pervasive circadian rhythm disruptor, artificial light at night (ALAN), increased inflammation and altered angiogenic transcripts in the hippocampi of mice. Here, we examined the effects of four nights of ALAN exposure on mouse hippocampal vascular networks. To do this, we analyzed 2D and 3D images of hippocampal vasculature and hippocampal transcriptomic profiles of mice exposed to ALAN. ALAN reduced vascular density in the CA1 and CA2/3 of female mice and the dentate gyrus of male mice. Network structure and connectivity were also impaired in the CA2/3 of female mice. These results demonstrate the rapid and potent effects of ALAN on cerebrovascular networks, highlighting the importance of ALAN mitigation in the context of health and cerebrovascular disease.

INTRODUCTION

The function of the cardiovascular system is coordinated across the day by circadian rhythms.[1] Circadian rhythms are endogenously driven cyclical processes with periods of about 24 h (hence *circa*: about, *diem*: a day). These rhythms regulate and optimize the timing of various behavioral, physiological, and cellular processes in response to fluctuating energetic resource availability and the need for periods of rest.[2] Proper alignment and integrity of circadian rhythms are vital for cardiovascular health.[1]

Cardiovascular circadian rhythms are generated and modulated across the day by both rhythms within the cardiovascular system and by rhythmic humoral and neuronal signaling cues that act on the cardiovascular system.[2] For example, in mice, myocardial oxidative metabolism varies across the day in response to varying systemic energetic demands during sleep/wake activity.[3] Aortic tight-junction and extracellular matrix transcriptomic profiles also vary across the day, including rhythmic variation in genes such as claudin-5, junctional adhesion molecule-1, and elastin.[4] Circadian rhythms regulate several other cardiovascular processes, including vascular tone,[5] blood pressure,[6] heart rate,[7] and angiogenesis.[8] The coordination of many of these processes is necessary for responding to and recovering from varying energetic needs across the day.[2]

Alignment of internal circadian rhythms to the external environment is vital for health.[9] This alignment primarily occurs by solar light-dark signaling cues. Disruption of circadian rhythms leads to many negative physiological and behavioral consequences. Of the many circadian rhythm disruptors present in our modern environments, artificial light at night (ALAN) is the most pervasive.[10] ALAN affects a growing 80% of the global human population; this metric exceeds 99% in the US and Europe.[11] Circadian rhythm disruption caused by ALAN exposure has detrimental effects on the cardiovascular system.[12]

Previous evidence has demonstrated the rapid consequences of short-term exposure to ALAN.[13] Mice exposed to just four nights of ALAN exhibited increased neuroinflammation, increased depressive-like behavior, and importantly, altered angiogenic transcript profiles in the hippocampus.[13] Female and male mice exposed to as few as four nights of 5 lux of ALAN exhibited reduced hippocampal VEGF-A expression and elevated *Vegfr-1* expression, indicating disrupted angiogenic signaling.[13] VEGF-A is a

[1]Department of Neuroscience, Rockefeller Neuroscience Institute West Virginia University Morgantown, WV 26505, USA

[2]Department of Medicine, Division of Oncology/Hematology West Virginia University Morgantown, WV 26505, USA

[3]WVU Cancer Institute West Virginia University Morgantown, WV 26505 USA

[4]Lead contact

*Correspondence: jrbumgarner@mix.wvu.edu

https://doi.org/10.1016/j.isci.2023.106996

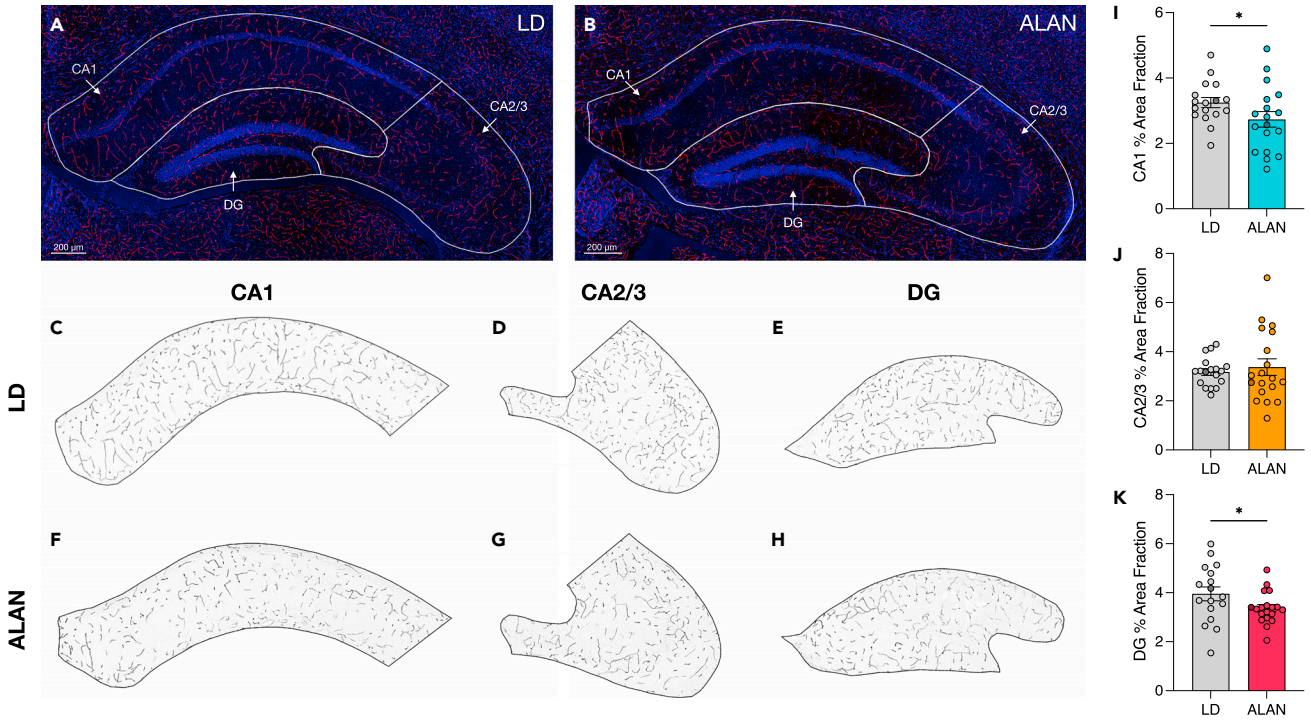

Figure 1. ALAN exposure reduces lectin percent area fraction in hippocampal CA1 and DG

(A and B) Lectin perfusion enabled the visualization and segmentation of the CA1, CA2/3, and dentate gyrus (DG) of the hippocampus of male and female mice exposed to either LD (C-E) or artificial light at night (F-H).

(I–K) Percent area fraction was calculated and compared in the CA1 (I), CA2/3 (J), and the DG (K) (n = 9 females/group, n = 9–10 males/group). Data were analyzed with a one-tailed *t*-test, as supported by an *a priori* hypothesis generated from evidence by Walker et al., 2020. Scale bars represent 200 µm. Data are represented as mean ± SEM. *p < 0.05.

potent angiogenic signaling factor[14]; reduction of VEGF-A signaling can reduce vascular density and alter vascular function.[15,16] Moreover, VEGFR-1 is capable of potentiating angiogenesis,[17] but also can sequester VEGF-A and inhibit angiogenesis.[18]

Based on this evidence, we hypothesized that four nights of exposure to 5 lux of ALAN alters vascular structure in the hippocampus of CFW mice. We tested this hypothesis by examining 2D sections of lectin-labeled hippocampal vasculature, large-scale 3D reconstructions of hippocampal vasculature generated with corrosion casting, and hippocampal bulk-sequencing transcriptome profiling.

RESULTS

ALAN alters hippocampal vascular density

To assess the effects of short-term ALAN exposure (4 nights) on hippocampal vascularity, we first perfused fluorescently labeled lectin, a carbohydrate-binding protein used to label vasculature. Following imaging, the CA1, CA2/3, and dentate gyrus (DG) of the hippocampus were manually segmented to examine the percent area fraction (PAF) of lectin staining (Figures 1A–1H). There were no sex differences in lectin PAF (see Summary Table), so the results between sexes were combined for subsequent lectin analyses. Reduced vascular density was observed in both the CA1 (Figure 1I) and DG (Figure 1K) of mice exposed to ALAN, supporting the hypothesis that ALAN disrupts cerebrovascular structure. Segmented lectin percent area fraction was not significantly different in the CA2/3 of mice exposed to ALAN (Figure 1J).

ALAN exposure alters the density of small-to-medium vessels in the hippocampus

Following the observation of reduced lectin-labeled vascular density, we sought to comprehensively examine the effects of ALAN on region-wide hippocampal vascular networks. To do this, cerebrovasculature casts were created using a corrosion casting procedure and were imaged using µCT.[19] This enabled

the 3D segmentation of the CA1, CA2/3, and DG for subsequent quantification of numerous vascular characteristics.

Vascular networks can be characterized by examining the whole-network topology and the mean features of individual segments.[20] First, the density of hippocampal vascularization by varying radii of vessels per mm^3 of tissue was examined in all three segmented regions. Female and male groups were separated in the subsequent analyses because of sex differences in several vascular features across the examined regions (e.g., Figures 3A–3C, S2). In both the CA1 (Figure 2A; $n_{females}$ = 7–8, n_{males} = 5–7) and the CA2/3 (Figure 2B) of female mice exposed to ALAN, the density of vessels with radii of 4–7 μm was reduced. Similarly, ALAN exposure reduced the density of 3–6 μm radius vessels in the DG of male mice (Figure 2F; Video S1). In the female CA1 and CA2/3 as well as the DG of male mice exposed to ALAN, there was an interaction between exposure to ALAN and the size of vessels that were reduced. There were no reductions in the vascular density in the DG of female mice (Figure 2C) or the CA1 or CA2/3 of male mice exposed to ALAN (Figures 2D and 2F).

ALAN alters network structure and topology in the CA2/3 of female mice

To further understand the effects of ALAN on whole-network vascular characteristics, we examined network volume and surface area in the corrosion casting μCT datasets. To do this, dorsal hippocampal vasculature was manually segmented, as described in the methods. In the CA2/3 of female mice, ALAN reduced total network volume (Figure 3A) and the total network surface (Figure 3B) area per mm^3 of segmentation volume. Volume and surface area differences were not observed in the CA1 or DG of either sex exposed to ALAN (Figure S1). Next, the effects of ALAN on the mean characteristics of individual segments were examined. ALAN increased the mean tortuosity (Figure S2F) and reduced the mean radius (Figure S2H) of vessels in the CA2/3 of female mice. No other alterations in individual segment characteristics were observed (Figure S2). Lastly, to examine the effects of ALAN on vascular network topology, we examined branchpoint and endpoint density as metrics of connectivity. ALAN exposure reduced network branchpoint density (Figure 3C) and increased endpoint density (Figure 3D) in the CA2/3 of female mice. These effects were not observed in any male hippocampal regions or the CA1 or DG of female mice (Figure S1).

ALAN alters hippocampal vascular transcriptomic profiles

Finally, to gain initial insight into the mechanisms by which ALAN exposure leads to altered hippocampal vasculature, we performed bulk-tissue RNA-sequencing on hippocampal dissections of mice exposed to four nights of ALAN. Several hundred differentially expressed genes were observed (Figures 4A and 4B), with minor overlap between sexes (Figure 4C). In females, we observed alterations in gene ontologies associated with extracellular matrix maintenance and organization, which included upregulated *Bmp7* and downregulated, *Col4a4*, *Col20a1*, and *Lamc2*, *Lama2*, among others (Figures 4D and 4F). Additional alterations in genes associated with angiogenesis were also observed in females exposed to ALAN, including downregulated *Nid1* and *Ctsg*. In male mice exposed to ALAN, we observed alterations of gene ontologies associated with blood vessel morphogenesis, angiogenesis, and blood-brain barrier maintenance, including upregulated *Fgfr2*, *Anxa2*, and *Mcam* and downregulated *Notch4, Coro1c*, and *Klf4* (Figure 4G).

DISCUSSION

The present study demonstrates that exposure to ALAN on a short timescale can rapidly alter the structure and density of vasculature in the hippocampus of male and female mice. Our preliminary analysis of vascular density using lectin perfusion indicates reduced vascularity in both the CA1 and the DG of the hippocampus. Following this preliminary analysis, 3D hippocampal vascular network alterations following exposure to ALAN were examined using corrosion casting. 3D structural analysis revealed that ALAN reduces the density of small-to-medium sized vessels in the CA1 and CA2/3 of female mice and the DG of male mice. Moreover, in the CA2/3 of female mice, ALAN reduces vascular volume and surface area, increases vessel tortuosity, and alters network topology as indicated by decreased branchpoint and increased endpoint density. Follow-up examination of hippocampal transcriptome profiles indicates altered gene patterns associated with vascular morphogenesis and extracellular matrix organization.

The evidence presented in this study is consistent with several lines of work that demonstrate that circadian rhythm disruption can directly impair vascular structure and function.[21] For example, rats exposed to dim

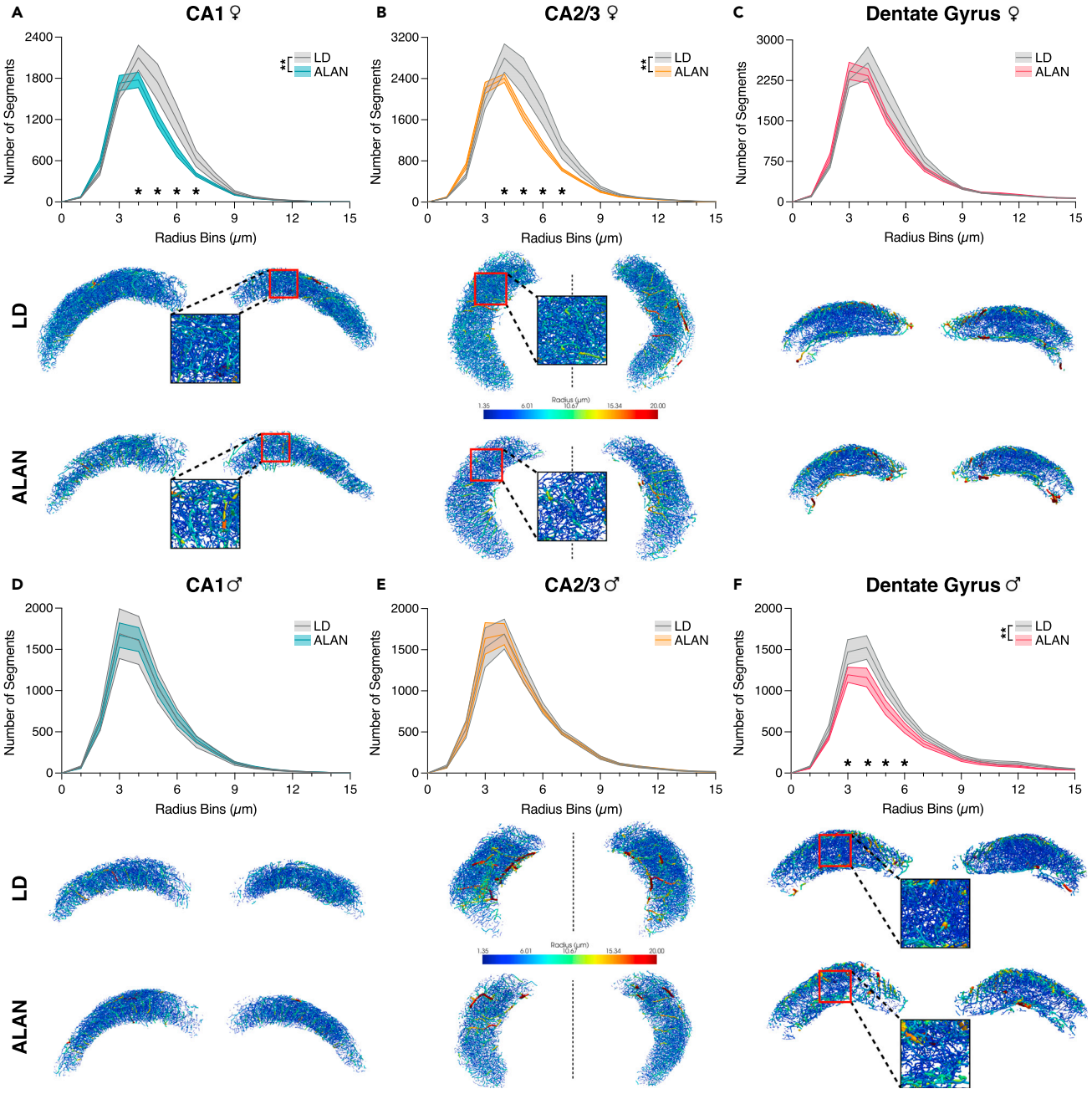

Figure 2. ALAN alters the density of small-to-medium-sized vessels in the hippocampus of female and male mice

(A–F) Vessel density by radius bins was assessed in female hippocampal CA1 (A), CA2/3 (B), and DG (C) and in male hippocampal CA1 (D), CA2/3 (E), and DG (F) (n = 7–8 females/group, n = 5–7 males/group). Data were analyzed using a two-way ANOVA with ALAN and radius size as the main effects. Sexes were analyzed separately. The dentate gyri in F have a scale bar from 1.35–25.0 μm. Data are represented as mean ± SEM. *p < 0.05, **p < 0.01.

ALAN at levels of 1–2 lux for 5 weeks exhibited reduced nocturnal systolic blood pressure, altered heart rate rhythms, and altered cardiovascular responses to norepinephrine.[22] In the same study, exposure to ALAN for 2 weeks elevated aortic expression of endothelial nitric oxide synthase.[22] Similar cardiovascular disruption is observed in spontaneously hypertensive rats exposed to dim ALAN.[23] ALAN exposure increased systolic blood pressure and reduced systolic blood pressure variability.[23] Humans exposed to a 3-day simulated shift work paradigm exhibited elevated both systolic and diastolic blood pressure as well as reduced nocturnal systolic blood pressure dipping.[24]

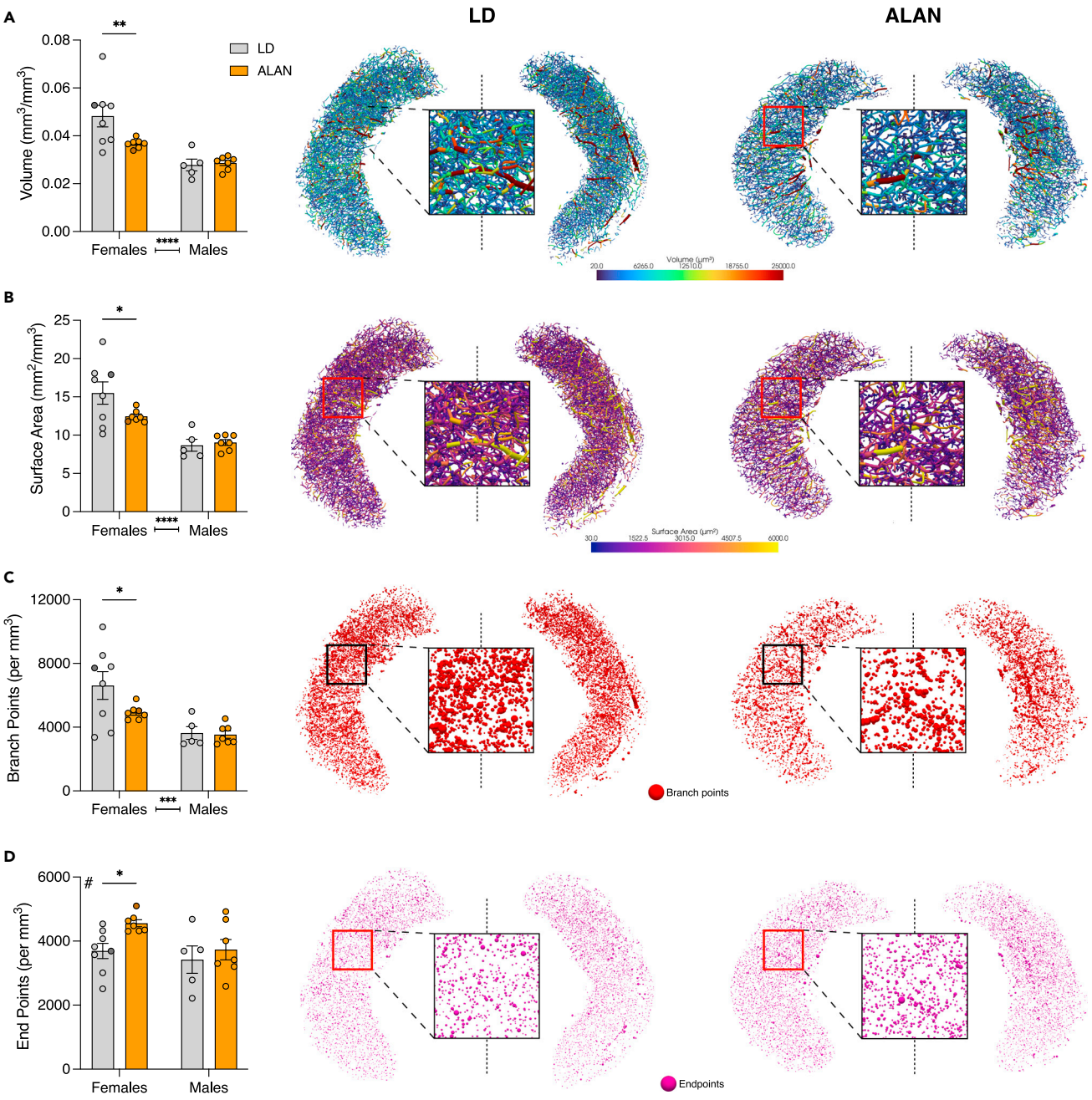

Figure 3. ALAN alters the structure and topological features of the CA2/3 in female mice

(A–D) The effects of ALAN on network volume (A) and surface area (B) were examined. Network connectivity was also assessed by examining branchpoint (C) and endpoint density (D) (n = 7–8 females/group, n = 5–7 males/group). Data were analyzed using a two-way ANOVA and planned multiple comparisons within sex were made using Fisher's LSD. # - Main effect of lighting condition. Data are represented as mean ± SEM. *p < 0.05, **p < 0.01, ***p < 0.001, ****p < 0.0001.

In the context of cardiovascular pathology, a week of exposure to ALAN in a rodent model of cerebral ischemia led to increased mortality, neuroinflammation, and Iba1 immunoreactivity, a marker for activated microglia/macrophages.[25] Moreover, a single night of ALAN exposure increases infarct penumbral volume following experimental stroke in mice.[26] Other work has demonstrated that Per2 is necessary for the proper function of endothelial progenitor cells following myocardial infarction in mice, although cell function was examined *in vitro*.[27]

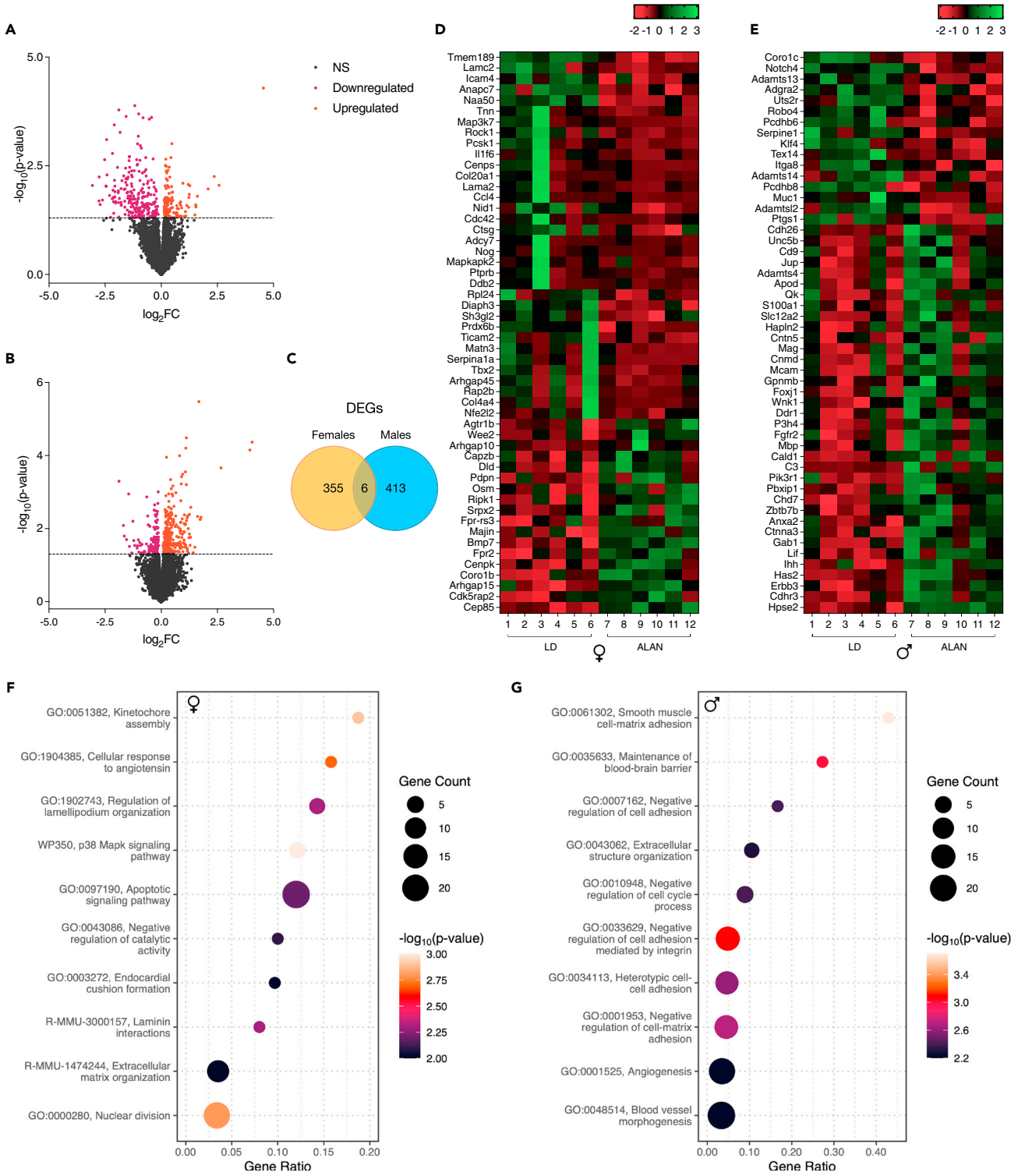

Figure 4. ALAN exposure alters gene expression related to angiogenesis, extracellular matrix composition, and blood-brain-barrier integrity

(A and B) Volcano plots visualizing differentially the results of the sequencing analyses.

(C) Venn diagram showing overlap of differentially expressed genes between sexes.

(D and E) Heatmaps visualizing differentially expressed genes tied to relevant extracellular matrix organization, blood vessel morphogenesis, or angiogenesis pathways.

(F and G) Gene ontology bubble plots demonstrating significantly altered biological pathways (n = 6 animals/group).

Previous research examining the effects of ALAN on zebra finch physiology has demonstrated hippocampal-specific and sex-differential effects. One study noted that female zebra finch exposed to 5 lux of ALAN for 7 weeks exhibited increased neuronal recruitment to the medial striatum, hippocampus, and the nidopallium caudale. However, ALAN only increased total neuronal density in the hippocampus, highlighting a hippocampal-specific effect of ALAN.[28] A follow-up study examining ALAN exposure on male zebra finches observed that ALAN increased neuronal recruitment in several other structures, but not the hippocampus. In contrast to the observed results in females, ALAN did not increase neuronal density or neuronal recruitment in the hippocampus of male zebra finches after six weeks of 5 lux of ALAN exposure.[29] Notably, ALAN exposure did alter neuronal recruitment and density in other brain regions.[29] These region- and sex-specific effects of ALAN on hippocampal neuronal characteristics are tangential but complementary to the effects observed in the present study.

ALAN exposure may also have indirectly induced the vascular structural alterations observed in this study via inflammation. ALAN exposure induces states of neuroinflammation in humans and other species,[30] and inflammation is associated with vascular remodeling.[31–33] Siberian hamsters exposed to ALAN exhibit elevated hippocampal *Tnf*.[34] Male mice exposed to ALAN exhibit elevated hippocampal *Tnf* and *Il-6*[35] as well as medullar *Il-6*.[36] Moreover, in the context of the short-term scale of ALAN exposure demonstrated in this study, our previous work demonstrated that only 3 nights of exposure to 5 lux of ALAN increased hippocampal *Il-1β* in female mice.[13] Elevated neuroinflammation may be a determining factor for the presence of altered cerebral vascular structure in this study, as adult angiogenesis is thought to primarily be driven by inflammation.[33] Future work may seek to examine inflammatory alterations and their relation to vascular structure and remodeling.

Angiogenesis and vascular remodeling are regulated by clock genes, directly implicating the ability for circadian rhythm disruption to alter vascular structure.[37] Indeed, circadian transcription factor binding sites, including E-boxes, D-boxes, F-boxes, and ROREs are present in the promoter regions of numerous angiogenic proteins.[8] Disruption of the clock gene expression loop can alter vascular development in zebrafish.[38,39] An *in vitro* assessment of angiogenesis demonstrated that clock synchronization of pericytes and endothelial cells increased tube formation and endothelial cell counts relative to desynchronized cells, further implicating the circadian clock in vascular remodeling.[40] Further, Bmal1 knockout mice exhibit pathological carotid artery vascular remodeling.[41] Lastly, as previously noted and as supported by our transcriptomic results, ALAN can alter angiogenic signaling in mice.[13]

The observed regional sex differences in vascular network alterations may be a result of underlying sex differences in cardiovascular circadian rhythms[42] or sex differences in the effects of circadian rhythm disruption.[43] For example, there are sex differences in basal cardiovascular tone[44] and heart rate variability,[45] and these differences persist when examined across the day.[46–49] Sex differences in inflammatory responses and immune function following ALAN exposure have also been previously noted.[13,50,51] Sex differences in angiogenic transcript alterations in the hippocampus following ALAN exposure have also been reported.[13] As noted, VEGF-A was decreased in both sexes, but *Vegfr-1* was only increased in female hippocampal tissue.[13] Of note, the observed sex differences were only detected in the 3D casting data. This is likely because, in contrast to 2D lectin staining, network analysis with 3D can detect fine-grained differences in vasculature.[19] Lastly, the observed sex differences may also be an effect of circulating estrogen, as estrogen does play a role vascular reactivity[52] and vascular remodeling.[53]

Future work may seek to directly examine the effects of restoring hippocampal vascularization on hippocampal function, for example via intraventricular infusion of VEGF. To assess the contribution of female sex hormones to the observed sex differences in ALAN-induced hippocampal vascular alterations, future experiments may examine effects in ovariectomized mice or stratify female mice by estrus phase for vascular structure comparisons.

The present study provides further insight into a growing body of work relating disrupted circadian rhythms and impaired cardiovascular function. The effects of ALAN exposure on cerebrovascular structure on such a rapid timescale highlight the continuing need to consider ALAN as a dangerous and pervasive circadian rhythm disruptor.

Limitations of study

There are several limitations present in this study. An important limitation is that the presented evidence is primarily characteristic and correlative in the context of previously published results. Next, the vascular characterizations in this study were conducted *ex vivo*, preventing inferences about blood flow dynamics and real-time insights into vascular remodeling. A further limitation was our narrowed examination of dorsal hippocampal vascular alterations because of the limitations of our manual structure segmentation from the 3D reconstructions. Future work may seek to examine vascular alterations using 3D LSFM approaches that allow for automatic region registration and segmentation. Moreover, we did not directly examine the concentration of circulating sex hormones to determine their potential role in the underlying observed sex differences. A final noted limitation of this study was the single timepoint examination of the effects of ALAN on hippocampal vascular structure. Future multi-timepoint examinations may elucidate whether there are underlying circadian differences in structural alterations that are disrupted by ALAN exposure.

STAR★METHODS

Detailed methods are provided in the online version of this paper and include the following:

- KEY RESOURCES TABLE
- RESOURCE AVAILABILITY
  - Lead contact
  - Materials availability
  - Data and code availability
- EXPERIMENTAL MODEL AND STUDY PARTICIPANT DETAILS
  - Animals
- METHOD DETAILS
  - Resin perfusions
  - μCT scanning
  - RNA-sequencing
  - Tomato lectin perfusion and lectin analysis
- QUANTIFICATION AND STATISTICAL ANALYSIS

SUPPLEMENTAL INFORMATION

Supplemental information can be found online at https://doi.org/10.1016/j.isci.2023.106996.

ACKNOWLEDGMENTS

We thank Evan McCray for his guidance on the design of the figures. The graphical abstract was created with BioRender.com. The authors were supported by grants from NINDS (R01NS092388 to RJN and ACD), NCCIH (R21AT011238-01 to RJN), and NIGMS award number 5U54GM104942. The content is solely the responsibility of the authors and does not necessarily represent the official views of the National Institutes of Health.

AUTHOR CONTRIBUTIONS

J.R.B., W.H.W. II, A.C.D., and R.J.N. conceived the idea and aims of the manuscript. J.R.B., D.D.Q., R.C.W, A.A.R., and J.A.L., acquired and analyzed the 3D corrosion casting data. J.R.B., W.H.W. II, and O.H.M.F acquired and analyzed the lectin data. J.R.B., D.D.B.K., and J.C.W. acquired and analyzed the RNA-seq data. J.R.B. and R.J.N. wrote the manuscript. All authors discussed the results and consulted on the manuscript.

DECLARATION OF INTERESTS

The authors declare no competing interests.

INCLUSION AND DIVERSITY

We support inclusive, diverse, and equitable conduct of research.

Received: October 20, 2022
Revised: March 15, 2023
Accepted: May 25, 2023
Published: May 29, 2023

REFERENCES

1. Thosar, S.S., Butler, M.P., and Shea, S.A. (2018). Role of the circadian system in cardiovascular disease. J. Clin. Invest. *128*, 2157–2167.

2. Rana, S., Prabhu, S.D., and Young, M.E. (2020). Chronobiological influence over cardiovascular function: the good, the bad, and the ugly. Circ. Res. *126*, 258–279.

3. Young, M.E., Razeghi, P., Cedars, A.M., Guthrie, P.H., and Taegtmeyer, H. (2001). Intrinsic diurnal variations in cardiac metabolism and contractile function. Circ. Res. *89*, 1199–1208.

4. Rudic, R.D., McNamara, P., Reilly, D., Grosser, T., Curtis, A.M., Price, T.S., Panda, S., Hogenesch, J.B., and FitzGerald, G.A. (2005). Bioinformatic analysis of circadian gene oscillation in mouse aorta. Circulation *112*, 2716–2724.

5. Panza, J.A., Epstein, S.E., and Quyyumi, A.A. (1991). Circadian variation in vascular tone and its relation to alpha-sympathetic vasoconstrictor activity. N. Engl. J. Med. *325*, 986–990.

6. Douma, L.G., and Gumz, M.L. (2018). Circadian clock-mediated regulation of blood pressure. Free Radic. Biol. Med. *119*, 108–114.

7. Black, N., D'Souza, A., Wang, Y., Piggins, H., Dobrzynski, H., Morris, G., and Boyett, M.R. (2019). Circadian rhythm of cardiac electrophysiology, arrhythmogenesis, and the underlying mechanisms. Heart Rhythm *16*, 298–307.

8. Jensen, L.D., Gyllenhaal, C., and Block, K. (2014). Circadian angiogenesis. Biomol. Concepts *5*, 245–256.

9. Walker, W.H., Walton, J.C., DeVries, A.C., and Nelson, R.J. (2020). Circadian rhythm disruption and mental health. Transl. Psychiatry *10*, 28.

10. Bumgarner, J.R., and Nelson, R.J. (2021). Light at night and disrupted circadian rhythms alter physiology and behavior. Integr. Comp. Biol. icab017.

11. Falchi, F., Cinzano, P., Duriscoe, D., Kyba, C.C.M., Elvidge, C.D., Baugh, K., Portnov, B.A., Rybnikova, N.A., and Furgoni, R. (2016). The new world atlas of artificial night sky brightness. Sci. Adv. *2*, e1600377.

12. Meléndez-Fernández, O.H., Walton, J.C., DeVries, A.C., and Nelson, R.J. (2021). Clocks, rhythms, sex, and hearts: how disrupted circadian rhythms, time-of-day, and sex influence cardiovascular health. Biomolecules *11*, 883.

13. Walker, W.H., Borniger, J.C., Gaudier-Diaz, M.M., Hecmarie Meléndez-Fernández, O., Pascoe, J.L., Courtney DeVries, A., and Nelson, R.J. (2020). Acute exposure to low-level light at night is sufficient to induce neurological changes and depressive-like behavior. Mol. Psychiatr. *25*, 1080–1093.

14. Duffy, A.M., Bouchier-Hayes, D.J., and Harmey, J.H. (2004). Vascular endothelial growth factor (VEGF) and its role in non-endothelial cells: autocrine signalling by VEGF. In VEGF and Cancer, J.H. Harmey, ed. (Kluwer Academic/Plenum Publishers), pp. 133–144.

15. Olfert, I.M., Howlett, R.A., Tang, K., Dalton, N.D., Gu, Y., Peterson, K.L., Wagner, P.D., and Breen, E.C. (2009). Muscle-specific VEGF deficiency greatly reduces exercise endurance in mice. J. Physiol. *587*, 1755–1767.

16. Gharakhanian, R., Su, S., and Aprahamian, T. (2019). Vascular endothelial growth factor-a deficiency in perivascular adipose tissue impairs macrovascular function. Front. Physiol. *10*, 687.

17. Park, K., Amano, H., Ito, Y., Kashiwagi, S., Yamazaki, Y., Takeda, A., Shibuya, M., Kitasato, H., and Majima, M. (2016). Vascular endothelial growth factor receptor-1 (VEGFR-1) signaling enhances angiogenesis in a surgical sponge model. Biomed. Pharmacother. *78*, 140–149.

18. Kikuchi, R., Stevens, M., Harada, K., Oltean, S., and Murohara, T. (2019). Anti-angiogenic isoform of vascular endothelial growth factor-a in cardiovascular and renal disease. Adv. Clin. Chem. *88*, 1–33.

19. Quintana, D.D., Lewis, S.E., Anantula, Y., Garcia, J.A., Sarkar, S.N., Cavendish, J.Z., Brown, C.M., and Simpkins, J.W. (2019). The cerebral angiome: high resolution microct imaging of the whole brain cerebrovasculature in female and male mice. Neuroimage. *202*, 116109.

20. Kirst, C., Skriabine, S., Vieites-Prado, A., Topilko, T., Bertin, P., Gerschenfeld, G., Verny, F., Topilko, P., Michalski, N., Tessier-Lavigne, M., and Renier, N. (2020). Mapping the fine-scale organization and plasticity of the brain vasculature. Cell *180*, 780–795.e25.

21. Chellappa, S.L., Vujovic, N., Williams, J.S., and Scheer, F.A.J.L. (2019). Impact of circadian disruption on cardiovascular function and disease. Trends Endocrinol. Metabol. *30*, 767–779.

22. Molcan, L., Sutovska, H., Okuliarova, M., Senko, T., Krskova, L., and Zeman, M. (2019). Dim light at night attenuates circadian rhythms in the cardiovascular system and suppresses melatonin in rats. Life Sci. *231*, 116568.

23. Rumanova, V.S., Okuliarova, M., Molcan, L., Sutovska, H., and Zeman, M. (2019). Consequences of low-intensity light at night on cardiovascular and metabolic parameters in spontaneously hypertensive rats. Can. J. Physiol. Pharmacol. *97*, 863–871.

24. Morris, C.J., Purvis, T.E., Hu, K., and Scheer, F.A.J.L. (2016). Circadian misalignment increases cardiovascular disease risk factors in humans. Proc. Natl. Acad. Sci. USA *113*, E1402–E1411.

25. Fonken, L.K., Bedrosian, T.A., Zhang, N., Weil, Z.M., DeVries, A.C., and Nelson, R.J. (2019). Dim light at night impairs recovery from global cerebral ischemia. Exp. Neurol. *317*, 100–109.

26. Weil, Z.M., Fonken, L.K., Walker, W.H., Bumgarner, J.R., Liu, J.A., Melendez-Fernandez, O.H., Zhang, N., DeVries, A.C., and Nelson, R.J. (2020). Dim light at night exacerbates stroke outcome. Eur. J. Neurosci. *52*, 4139–4146.

27. Sun, Y.Y., Bai, W.W., Wang, B., Lu, X.T., Xing, Y.F., Cheng, W., Liu, X.Q., and Zhao, Y.X. (2014). Period 2 is essential to maintain early endothelial progenitor cell function in vitro and angiogenesis after myocardial infarction in mice. J. Cell Mol. Med. *18*, 907–918.

28. Moaraf, S., Heiblum, R., Vistoropsky, Y., Okuliarová, M., Zeman, M., and Barnea, A. (2020). Artificial light at night increases recruitment of new neurons and differentially affects various brain regions in female zebra finches. Int. J. Mol. Sci. *21*, 6140.

29. Moaraf, S., Heiblum, R., Okuliarová, M., Hefetz, A., Scharf, I., Zeman, M., and Barnea, A. (2021). Evidence that artificial light at night induces structure-specific changes in brain plasticity in a diurnal bird. Biomolecules *11*, 1069.

30. Walker, W.H., Bumgarner, J.R., Becker-Krail, D.D., May, L.E., Liu, J.A., and Nelson, R.J. (2021). Light at night disrupts biological clocks, calendars, and immune function. Semin. Immunopathol. *44*, 165–173.

31. Intengan, H.D., and Schiffrin, E.L. (2001). Vascular remodeling in hypertension: roles of apoptosis, inflammation, and fibrosis. Hypertension *38*, 581–587.

32. Muramatsu, R., Takahashi, C., Miyake, S., Fujimura, H., Mochizuki, H., and Yamashita, T. (2012). Angiogenesis induced by cns inflammation promotes neuronal remodeling through vessel-derived prostacyclin. Nat. Med. *18*, 1658–1664.

33. Pearson-Leary, J., Eacret, D., Chen, R., Takano, H., Nicholas, B., and Bhatnagar, S. (2017). Inflammation and vascular remodeling in the ventral hippocampus contributes to

vulnerability to stress. Transl. Psychiatry *7*, e1160.

34. Bedrosian, T.A., Weil, Z.M., and Nelson, R.J. (2013). Chronic dim light at night provokes reversible depression-like phenotype: possible role for TNF. Mol. Psychiatr. *18*, 930–936.

35. Hogan, M.K., Kovalycsik, T., Sun, Q., Rajagopalan, S., and Nelson, R.J. (2015). Combined effects of exposure to dim light at night and fine particulate matter on C3H/HeNHsd mice. Behav. Brain Res. *294*, 81–88.

36. Bumgarner, J.R., Walker, W.H., Liu, J.A., Walton, J.C., and Nelson, R.J. (2020). Dim light at night exposure induces cold hyperalgesia and mechanical allodynia in male mice. Neuroscience *434*, 111–119.

37. Paschos, G.K., and FitzGerald, G.A. (2010). Circadian clocks and vascular function. Circ. Res. *106*, 833–841.

38. Jensen, L.D., Cao, Z., Nakamura, M., Yang, Y., Bräutigam, L., Andersson, P., Zhang, Y., Wahlberg, E., Länne, T., Hosaka, K., and Cao, Y. (2012). Opposing effects of circadian clock genes BMAL1 and PERIOD2 in regulation of VEGF-dependent angiogenesis in developing zebrafish. Cell Rep. *2*, 231–241.

39. Jensen, L.D., and Cao, Y. (2013). Clock controls angiogenesis. Cell Cycle *12*, 405–408.

40. Mastrullo, V., Van Der Veen, D.R., Gupta, P., Matos, R.S., Johnston, J.D., McVey, J.H., Madeddu, P., Velliou, E.G., and Campagnolo, P. (2022). Pericytes' circadian clock affect endothelial cells' synchronization and angiogenesis in a 3d tissue engineered scaffold. Front. Pharmacol. *785*.

41. Anea, C.B., Zhang, M., Stepp, D.W., Simkins, G.B., Reed, G., Fulton, D.J., and Rudic, R.D. (2009). Vascular disease in mice with a dysfunctional circadian clock. Circulation *119*, 1510–1517.

42. Walton, J.C., Bumgarner, J.R., and Nelson, R.J. (2022). Sex differences in circadian rhythms. Cold Spring Harbor Perspect. Biol. *14*, a039107.

43. Bailey, M., and Silver, R. (2014). Sex differences in circadian timing systems: implications for disease. Front. Neuroendocrinol. *35*, 111–139.

44. Merz, A.A., and Cheng, S. (2016). Sex differences in cardiovascular ageing. Heart *102*, 825–831.

45. Koenig, J., and Thayer, J.F. (2016). Sex differences in healthy human heart rate variability: a meta-analysis. Neurosci. Biobehav. Rev. *64*, 288–310.

46. O'Connor, M.F., Motivala, S.J., Valladares, E.M., Olmstead, R., and Irwin, M.R. (2007). Sex differences in monocyte expression of IL-6: role of autonomic mechanisms. Am. J. Physiol. Regul. Integr. Comp. Physiol. *293*, R145–R151.

47. Hermida, R.C., Ayala, D.E., Fernández, J.R., Mojón, A., Alonso, I., and Calvo, C. (2002). Modeling the circadian variability of ambulatorily monitored blood pressure by multiple-component analysis. Chronobiol. Int. *19*, 461–481.

48. Hermida, R.C., Ayala, D.E., and Portaluppi, F. (2007). Circadian variation of blood pressure: the basis for the chronotherapy of hypertension. Adv. Drug Deliv. Rev. *59*, 904–922.

49. Hermida, R.C., Ayala, D.E., Mojón, A., Fontao, M.J., Chayán, L., and Fernández, J.R. (2013). Differences between men and women in ambulatory blood pressure thresholds for diagnosis of hypertension based on cardiovascular outcomes. Chronobiol. Int. *30*, 221–232.

50. Cissé, Y.M., Russart, K.L.G., and Nelson, R.J. (2017). Parental exposure to dim light at night prior to mating alters offspring adaptive immunity. Sci. Rep. *7*, 45497.

51. Cissé, Y.M., Russart, K., and Nelson, R.J. (2020). Exposure to dim light at night prior to conception attenuates offspring innate immune responses. PLoS One *15*, e0231140.

52. Miller, V.M., and Duckles, S.P. (2008). Vascular actions of estrogens: functional implications. Pharmacol. Rev. *60*, 210–241.

53. Gros, R., Hussain, Y., Chorazyczewski, J., Pickering, J.G., Ding, Q., and Feldman, R.D. (2016). Extent of vascular remodeling is dependent on the balance between estrogen receptor α and g-protein–coupled estrogen receptor. Hypertension. *68*, 1225–1235.

54. Zhang, X., Yin, X., Zhang, J., Li, A., Gong, H., Luo, Q., Zhang, H., Gao, Z., and Jiang, H. (2019). High-resolution mapping of brain vasculature and its impairment in the hippocampus of alzheimer's disease mice. Natl. Sci. Rev. *6*, 1223–1238.

55. Bumgarner, J.R., and Nelson, R.J. (2022). Open-source analysis and visualization of segmented vasculature datasets with vesselvio. Cell Rep. Methods *2*, 100189.

56. Bolger, A.M., Lohse, M., and Usadel, B. (2014). Trimmomatic: a flexible trimmer for illumina sequence data. Bioinformatics *30*, 2114–2120.

57. Dobin, A., Davis, C.A., Schlesinger, F., Drenkow, J., Zaleski, C., Jha, S., Batut, P., Chaisson, M., and Gingeras, T.R. (2013). Star: ultrafast universal RNA-seq aligner. Bioinformatics *29*, 15–21.

58. Love, M.I., Huber, W., and Anders, S. (2014). Moderated estimation of fold change and dispersion for RNA-seq data with deseq2. Genome Biol. *15*, 550–621.

59. Schneider, C.A., Rasband, W.S., and Eliceiri, K.W. (2012). Nih image to ImageJ: 25 years of image analysis. Nat. Methods *9*, 671–675.

STAR★METHODS

KEY RESOURCES TABLE

REAGENT or RESOURCE	SOURCE	IDENTIFIER
Antibodies		
DyLight-594 tagged tomato (Lycopersicon esculentum) lectin	Vector Laboratories	DL-1177-1
Chemicals, peptides, and recombinant proteins		
Heparin Sulfate	McKesson Corporation	63739-931-28
Paraformaldehyde	Acros Organics	416780030
PU4ii Resin and Hardener	VasQTec	NA
Methyl Ethyl Ketone	Fisher Chemical	M209
Formic Acid	VWR International	BDH4554
Potassium Hydroxide	VWR International	BDH7622
Phosphate Buffered Saline	Gibco	10010-023
Osmium Tetroxide	Sigma Aldrich	75632
Isoflurane	VetOne	502017
Deposited data		
RNA Sequencing Results	Harvard Dataverse	https://doi.org/10.7910/DVN/5EKYEM
Statistical Analysis Summary Tables	Harvard Dataverse	https://doi.org/10.7910/DVN/C6QPR9
Experimental models: Organisms/strains		
Female and Male CFW Mice	Charles River Laboratories	#024
Software and algorithms		
microCT 3D.SUITE Software	Bruker	NA
Prism 9.3.0	GraphPad	https://www.graphpad.com/scientific-software/prism/
ImageJ 2.3.0	Schneider et al., 2012	https://imagej.nih.gov/ij/
VesselVio Application Downloads and Terminal-Build Instructions	Bumgarner and Nelson, 2022	https://jacobbumgarner.github.io/VesselVio/
Other		
Teklad Global 18% Protein Rodent Chow	Teklad	2018
Skyscan μCT Scanner	Bruker	1272
BZ-X710 microscope	Keyence	NA

RESOURCE AVAILABILITY

Lead contact

Further information and requests for resources related to this study should be directed to and will be fulfilled by the lead contact, Jacob Bumgarner (jrbumgarner@mix.wvu.edu).

Materials availability

This study did not generate new unique reagents.

Data and code availability

All RNA Sequencing data have been deposited at Harvard Dataverse and are publically available as of the date of publication. DOIs are listed in the key resources table. This paper does not report original code. Any additional information required to reanalyze the data reported in this paper is available from the lead contact upon request.

EXPERIMENTAL MODEL AND STUDY PARTICIPANT DETAILS

Animals

Adult female and male Swiss Webster (CFW) mice (7-8 weeks old; Charles River Laboratories) were obtained and given 1 week to acclimate to standard vivarium conditions (14:10 h light: dark; 150±25:0 lux, 22±2°C; 12.0 x 6.5 x 5.5" polycarbonate cages). Upon arrival, mice were housed in groups of five per cage. Following the acclimation period, mice were singly housed and randomly assigned to either the vivarium light-dark (LD) cycle or dim artificial light at night (ALAN; 14:10 h; 150±25: 5±1 lux) housing conditions with lights on at 05:00 h and off at 19:00 h. ALAN sources were Luma5 Standard LED light strips (1.5 W/ft, 5000K "cool white", 1200 lumens; Hitlights Inc.); lux calibrations were conducted by placing a Mavolux 5023C illuminance meter (Gossen) in the center of an empty cage with the light sensor facing towards the ceiling. After group assignment, the animals were placed in their respective lighting conditions for a total of four nights prior to lectin perfusion, corrosion casting, or tissue collection. Food (2018 Teklad; Envigo) and reverse osmosis water were provided *ad libitum* throughout the entire duration of the experiment. All studies were approved by the West Virginia University Institutional Animal Care and Use Committee, and animals were maintained in accordance with NIH Animal Welfare guidelines.

METHOD DETAILS

Resin perfusions

Between 12:00-16:00 h on the day following the 4th experimental night of LD or ALAN conditions, resin casting perfusions were conducted as described previously.[19] Prior to perfusion, animals were deeply anesthetized with isoflurane and injected intraperitoneally (i.p.) with 25 U of heparin (63739-931-28; McKesson Corporation) in 250 μL of saline. Following absence of a response to the pedal reflex tests (confirming deep anesthetization), mice were transcardially perfused at a flow rate of 4 mL/min first with 15 mL of 25U/mL heparin in saline and then with 15 mL of 4% paraformaldehyde dissolved in 1x PBS (#416780030; Acros Organics). Next, animals were perfused with PU4ii resin that was formulated as described by the manufacturer's guidelines (VasQTec). Experimental groups were stratified across multiple days of perfusions.

Five days following the resin perfusions, the craniums were dissected and decalcified with a 12 h wash of 5% formic acid (BDH4554; VWR International). The brains were then dissected, and the remaining tissue was removed from the casts with two 12 h washes of 7.5% KOH (BDH7622; VWR International) at 50ºC. Casts were rinsed with Milli-Q water and subsequently osmicated in 1% osmium tetroxide (#75632; Sigma Aldrich) for 12 h. Casts were then washed, frozen, and lyophilized prior to being mounted for μCT scanning.

μCT scanning

The resulting cerebrovascular casts were imaged on a SkyScan 1272 (Bruker) with the following parameters: 50 kV/ 200 μA with no filter; 360° rotation in step sizes of 0.17°; 900 ms exposures; 4 frame averages/step to produce an isotropic voxel resolution of 2.7 μm^3. Scans were reconstructed using NRecon (Bruker) with the following parameters: beam hardening corrections at 15%, ring artifact reduction at 3, smoothing at 0, custom alignment compensations set for each sample, and 0.02-0.40 dynamic image ranges. Scan and reconstruction parameters were determined based on the manufacturer's guidelines. Following reconstructions, the volumes were resliced coronally. Volumes were then loaded into CTAn (Bruker), and the dorsal hippocampal CA1, CA2/3, and dentate gyrus volumes between the approximate bregma -1.6 and -2.6 coordinates were manually segmented using the transverse hippocampal vessels and main vessels of the hippocampus[54] as intra- and inter-regional boundary guides alongside the p56 Allen Institute mouse brain atlas. Manual segmentations were interpolated at distances of 0.1 mm. Segmented vasculature volumes from the casting data were analyzed using VesselVio 1.1.1,[55] with a 10 μm filter for isolated segments and a 5 μm filter for endpoint segment pruning to account for skeletonization errors.

RNA-sequencing

Between 1200-1400 h on the day following the fourth night of experimental housing conditions, brains were collected from a separate cohort of mice. Following rapid cervical dislocation and decapitation, brains were dissected and stored in RNAlater at -80°C (Thermo Fisher) until subsequent hippocampal dissections. RNA was extracted from hippocampal tissue using TRIzol (Invitrogen), and the quantity and purity of RNA were examined using a NanoDrop One (Thermo Fisher). All samples had 260/280 nm absorption ratios above 1.8. Short-read paired-end 150 bp sequencing was conducted by Genewiz using Illumina HiSeq X machines, with a sufficiently high RNI integrity number (RIN) confirmed by Genewiz prior to sequencing.

Sequence reads were trimmed using Trimmomatic v.0.36,[56] and trimmed reads were mapped to the GRCm38 reference genome using STAR v.2.5.2b.[56,57] ENSEMBL gene ids were converted to gene symbols using biotools.fr. RNA-Seq data were analyzed using DESeq2.[58] Prior to analysis, lncRNA, miRNA, and pseudogenes were removed from the results list. Gene ontology and pathway analyses were conducted with Metascape.

Tomato lectin perfusion and lectin analysis

Mice were intravenously (tail vein) injected with 200 μL of DyLight-594 tagged tomato (Lycopersicon esculentum) lectin in 0.1 *M* PBS (0.5 mg/ml; Vector Laboratories). The lectin solution was allowed to circulate for 5 minutes, and then mice were given a lethal overdose of sodium pentobarbital followed by transcardial perfusion with ~50 ml 4% paraformaldehyde (PFA) in 0.1 *M* PBS. The brain was dissected and post-fixed overnight in fresh 4% PFA solution. Tissues were cryoprotected in 30% sucrose in 0.2 *M* phosphate buffer until sunk. Tissues were frozen on dry ice and then maintained at -80°C until sectioning. Tomato lectin injections and tissue collection occurred between 14:00 and 16:00 h.

Tissue was subsequently sectioned at 40 μm, and hippocampal regions between bregma -1.23 and -3.63 were imaged using a BZ-X710 microscope (Keyence). The images were loaded into ImageJ, and the RGB channels were split. The three hippocampal regions of interest – the CA1, CA2/3, and dentate gyrus (DG) – were then manually outlined on the DAPI channel (blue) with reference to the adult mouse Allen Brain Reference Atlas. Outlines were then applied to the lectin channel (red), which was thresholded using the default algorithm to measure percent area fraction of lectin staining. Percent area fractions were then weighted across the area of all sections for individual animals. Lectin image processing was conducted with FIJI v2.3.0.[59]

QUANTIFICATION AND STATISTICAL ANALYSIS

The CA1 & DG region lectin data were analyzed using unpaired *t*-tests and the CA2/3 region lectin data were analyzed with a Mann-Whitney test based on a non-normal distribution of data. The specific test used for the analysis of each region was determined by examining the normality of residuals as determined by the Shapiro-Wilk test and the similarity between variances as determined by F-test for variance. Outliers were detected in the lectin data using the Grubb's test; no more than one outlier was removed per group. All lectin perfusion tests were one-tailed based on our *a priori* hypothesis supported by previous evidence.[13] The vascular corrosion cast data were analyzed using 2-way ANOVAs; *a priori* planned comparisons between LD and ALAN conditions within sexes were made using Fisher's LSD. Outlier detection in the lectin vascular data was conducted using the Grubb's test; outliers were not examined in the casting data due to reduced sample sizes. Mean differences with p-values < 0.05 were considered statistically significant. All analyses were conducted using Prism 9 (GraphPad). All statistical results and analyses are available in the Summary Table uploaded to Harvard Dataverse; the DOI can be found in the key resources table.